Grain boundary segregation in metals*

P. Rama Rao

Atomic Energy Regulatory Board, Anushaktinagar, Mumbai 400 094, India and
Jawaharlal Nehru Centre for Advanced Scientific Research, Jakkur, Bangalore 560 064, India

With the help of Auger electron spectroscopy, grain boundary segregation isotherms have been determined in respect of several alloying and trace elements present in three power plant steels. The analysis of the isotherms yields information of immense value. Apart from delineating the kinetic stages in segregation and the interaction processes amongst the trace and alloying elements, the influence of solute elements, heat treatment practice and applied stress on the grain boundary segregation process, which in turn bears upon the material mechanical behaviour, becomes clear. The importance of this understanding is highlighted by the shop floor experience of processing advanced engineering steels, one case of which (17–4 PH stainless steel) is described in some detail. More recently has emerged an electronic basis for grain boundary cohesion in the presence of a segregant (P or B in Fe grain boundary). This is described in conclusion alongside a thermodynamic consideration of grain boundary embrittlement.

ADVANCES in technology facilitate design and development of complex engineering systems with enhanced performance capability. And reliability becomes an issue of concern. Reliability and durability of structural components in modern systems, e.g. high speed aircraft engines, nuclear power reactors and power plant turbines, are a matter for most serious attention. In this context, if someone were to ask the question, what is the most significant advance that has taken place in materials engineering, my answer would be: the coming together of the materials scientist and the mechanics engineer. Why does the one have to mesh with the other can be illustrated with several examples. The work presented[1] at the 1995 Annual Meeting of the Indian Academy of Sciences provides one. Here is another.

In mechanics, one deals with stress intensity factors and analyses fracture problems in terms of a critical value of the stress intensity beyond which flaws, inevitably present in a component, grow, link-up and propagate catastrophically. What is essential to appreciate is that, considerations such as those the mechanical engineer is used to apply can go completely awry in certain situations. That is where the materials scientist comes in. A classic situation[2], in this respect, is what happened in the Hinkley Point power station turbine generator (in 1969). During an overspeed test, the rotor of the turbine disintegrated. Scanning electron microscopic (SEM) examination of the fracture surface showed intergranular failure suggesting very little plastic deformation or energy expenditure. Auger electron spectroscopic (AES) analysis, then, pointed to the fact that the fracture surface was covered by 45% of a monolayer of *embrittling* P. Adsorption of submonolayer concentrations of elements at internal surfaces of engineering materials can be understood in terms of classical adsorption theories while the significance of AES lies in its ability to detect submonolayer concentrations, as in the foregoing case of failure, arising from segregation of a deleterious element to grain boundaries.

With enhancement factors of as much as 1000 for the segregants, grain boundary composition can be utterly distorted even when the bulk concentrations of the elements concerned are only a few parts per million. The detrimental effect of the segregating element was the cause of the turbine rotor failure and is reflected in a number of embrittling processes such as temper embrittlement, high temperature creep cavitation, stress relief cracking, stress corrosion cracking and so on.

The spectre of impurity elements looms large in the modern context especially because of two factors, one of which has to do with the complex chemistries of engineering alloys. Multicomponent systems are invariably being resorted to for making structural components of aircraft engines (e.g. nickel superalloys) or, for that matter, power plant turbines, as the examples of steels to be dealt with in this article will show. The second factor arises from the motivation to recycle materials, which is being increasingly practised to lower costs and to alleviate environmental damage. In these situations, if the common denominator of grain boundary segregation is understood and controlled, the engineer's ability to ensure reliability will have been substantially buttressed. This is the focus of the article.

We decided to investigate issues of segregation in multi-component engineering alloys (power plant steels with as many as 12 metal and metalloid additives to iron, Table 1). Some of the alloying additions are intentionally made while some are present as unavoidable trace impurities. These steels are interesting real-life materials because the extent of segregation can be exacerbated by co-segregation of minor alloying elements

*Based on the Presidential Address delivered at the 62nd Annual Meeting of the Indian Academy of Sciences held at Jodhpur, India, November 1–3, 1996.

Table 1. Chemical composition (wt%) of power plant steels

Steel	C	Ni	Cr	Mo	V	Si	Mn	P	S	N	Sb	Sn	Fe
12 CrMoV	0.22	0.42	11.27	0.42	0.2	0.35	0.42	0.012	0.01	0.006	–	0.038	bal
1.2 CrMoV	0.22	–	1.2	0.9	0.3	0.3	0.5	0.025	0.025	0.006	0.015	0.040	bal
NiCrMoV	0.24	2.6	0.40	0.28	0.1	0.24	0.34	0.01	0.01	0.006	–	0.04	bal

caused by significant mutual interaction. The approach taken to investigate these phenomena was through determination of segregation isotherms (to become clear in the following presentation). The knowledge thus gained is useful in solving practical (shop floor) problems which will be exemplified through case studies carried out at the Defence Metallurgical Research Laboratory, Hyderabad, principally by R. D. K. Misra and T. V. Balasubramanian. In conclusion will be summarized the attempts made to address the basic question: why should a given segregating element – an embrittler like P, or a cohesion enhancer like B – act in the manner observed at the grain boundary site?

Experimental method

For AES studies, fresh fracture surfaces are to be exposed. The steels that have been studied by us are amenable to meet this requirement. Fresh fracture surfaces, in these cases, can be obtained by impacting notched samples at liquid nitrogen temperature within the ultra high vacuum system of the AE specimen chamber. For the purpose of mapping segregation isotherms, cylindrical steel specimens (3.68 mm dia. × 320 mm long) were heat treated in the range 700–900 K.

A primary electron beam of 3 keV and a target current of 0.5 μA was used. A peak to peak amplitude of 3 eV at a frequency of 10 kHz was applied to the cylindrical mirror analyser for measurement of grain boundary chemistry. Some of the Auger electron peaks frequently analysed were Fe (703 eV), Ni (848 eV), Cr (529 eV), Sn (430 eV), N (379 eV) and C (272 eV).

The way the data are plotted is as follows. Intensity peak heights (H_x) of the various elements are normalized with respect to Fe. H_x can be converted into coverage, θ_x, of the particular element in the fracture surface, which is a measure of what per cent (%) of the monolayer is occupied by the segregating atoms at the grain boundary. (The procedure for conversion of H_x into θ_x was according to Seah[2].)

To examine the effect of applied stress, cylindrical tensile specimens were preloaded to 20 kg load (stress of 1.6 kg/mm^2) and then heated rapidly to the required test temperature at which the test load, say 465 kg (stress of 35 kg/mm^2) was applied manually. After the application of load for the required test duration, load was lifted and the specimen quenched to room temperature. Determination of grain boundary segregation isotherms followed via scanning Auger microprobe (SAM) on these stressaged samples machined to SAM specimen geometry in a manner similar to the above for unstressed specimens. The longitudinal direction of the SAM specimens always remained parallel to the direction of tensile loading. Descriptions of detailed experimental procedure for both stressed and unstressed specimens have been published[3–10].

Segregation isotherms

The information that the segregation isotherms yield is quite substantial. For the purpose of this article we shall select aspects pertaining to (a) kinetics of segregation and (b) interaction among alloying elements.

We shall then discuss selected steel processing problems that we have been able to resolve with the help of this type of investigations.

The three steels (Table 1) for which the segregation isotherms were determined, are power plant steels routinely used by Bharat Heavy Electricals Limited. Notice that the number of alloying elements in each case is more than ten. The *trace* elements, S, P, N, Sn, are common to all of them and these are important in our studies. This apart, two of the three steels, one of which has higher Cr (11.3%), are free of Ni. The third steel has 2.6% Ni. The three materials will thus allow us to examine the role of Cr and Ni.

Progress of segregation of the various elements, at a selected (773 K) constant temperature (isotherm), as a function of time of soaking at this temperature, is typically shown in Figure 1 *a*. Similar plots have been obtained at 823, 853 and 883 K. With respect to the steels used in the investigation, up to three stages have been observed (Figure 2). A summary of the kinetic stages is listed in Table 2.

Figure 1 *a* shows a parallel behaviour in the kinetics of segregation of N and Cr, suggesting Cr–N cooperative interaction. This type of interaction is marked by a constant ratio (θ_N/θ_{Cr}) of their coverage which is evident in Figure 1 *b*.

The cooperative interaction processes can be more complicated than the example in Figure 1 and may be governed by the compounds which the co-segregating elements are capable of forming (Figure 2). Thus, for the anticipated interaction between carbide and nitride-forming elements (Cr and V), $(\theta_N + \theta_C)/(\theta_{Cr} + \theta_V)$ is

plotted as a function of time in Figure 2 *b* and is observed to be time invariant at a value of 0.95.

It has been found useful to define a term called interaction severity, ϕ, which, for a cooperative elemental interaction during segregation, is expressed by the ratio of coverages, e.g. θ_N/θ_{Cr} as above, in respect of the interacting elements. ϕ for a site competitive process, on the other hand, would be expressed by a summation of the respective coverages, e.g. $(\theta_{Sn}+\theta_S)$, for the interacting elements Sn and S, as we can see in Figure 3. A value of $\theta_{Sn}+\theta_S=1$ would indicate a strong interactive process. This points to the advantage of looking at the ratios and the summations of coverage, ϕ, which is that the magnitude of ϕ can be used as a parameter to characterize the interaction process. The influence of crucial variables like temperature and microstructure would then be amenable for analysis in terms of variations of ϕ.

An interesting observation at higher ageing temperatures (853 K) pertains to the segregation of Ni and Sn (two substitutional solutes) which were, cooperatively coupled (Figure 2) in a manner similar to Cr and N (Figure 1). This is depicted by the constancy in the ratio, θ_{Sn}/θ_{Ni}, Figure 2 *c* (ref. 11). This type of Ni–Sn interaction has been seen in Mossbauer spectroscopy[12] and thermodynamically rationalized by Guttman[13] (Guttman's treatment will be briefly outlined subsequently). The Ni–Sn cooperative interaction, which can bring about an increased number of Ni nearest neighbours of Sn atoms or compound formation (Ni_3Sn or Ni_2Sn or Ni_3Sn_2), has been commented on

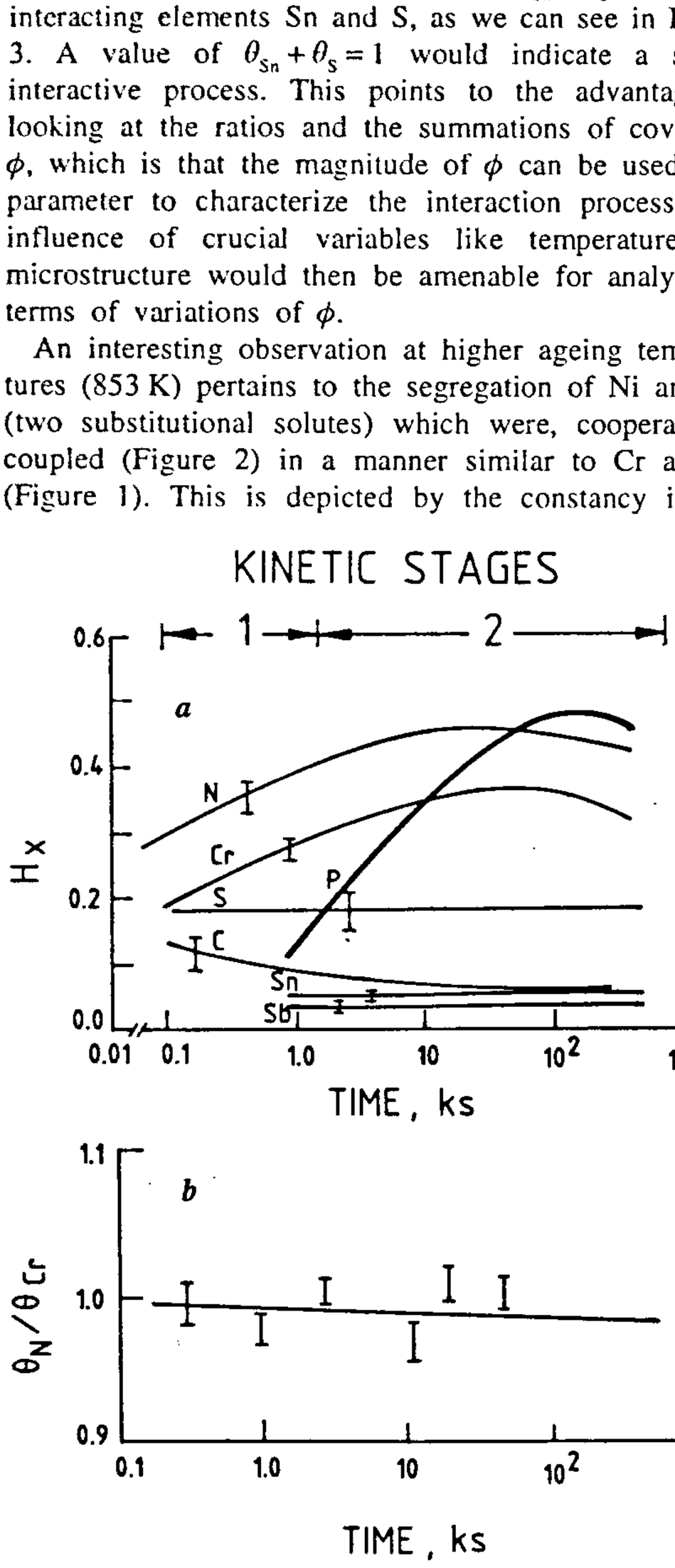

Figure 1. *a*, Grain boundary segregation isotherm at 773 K for 2.6% NiCrMoV powerplant steel. Bars indicate the range over which values were obtained (ref. 3). *b*, Time dependence of the ratio of coverages for the cooperatively interacting elements N and Cr, $\theta N/\theta Cr$ at 773 K (ref. 3).

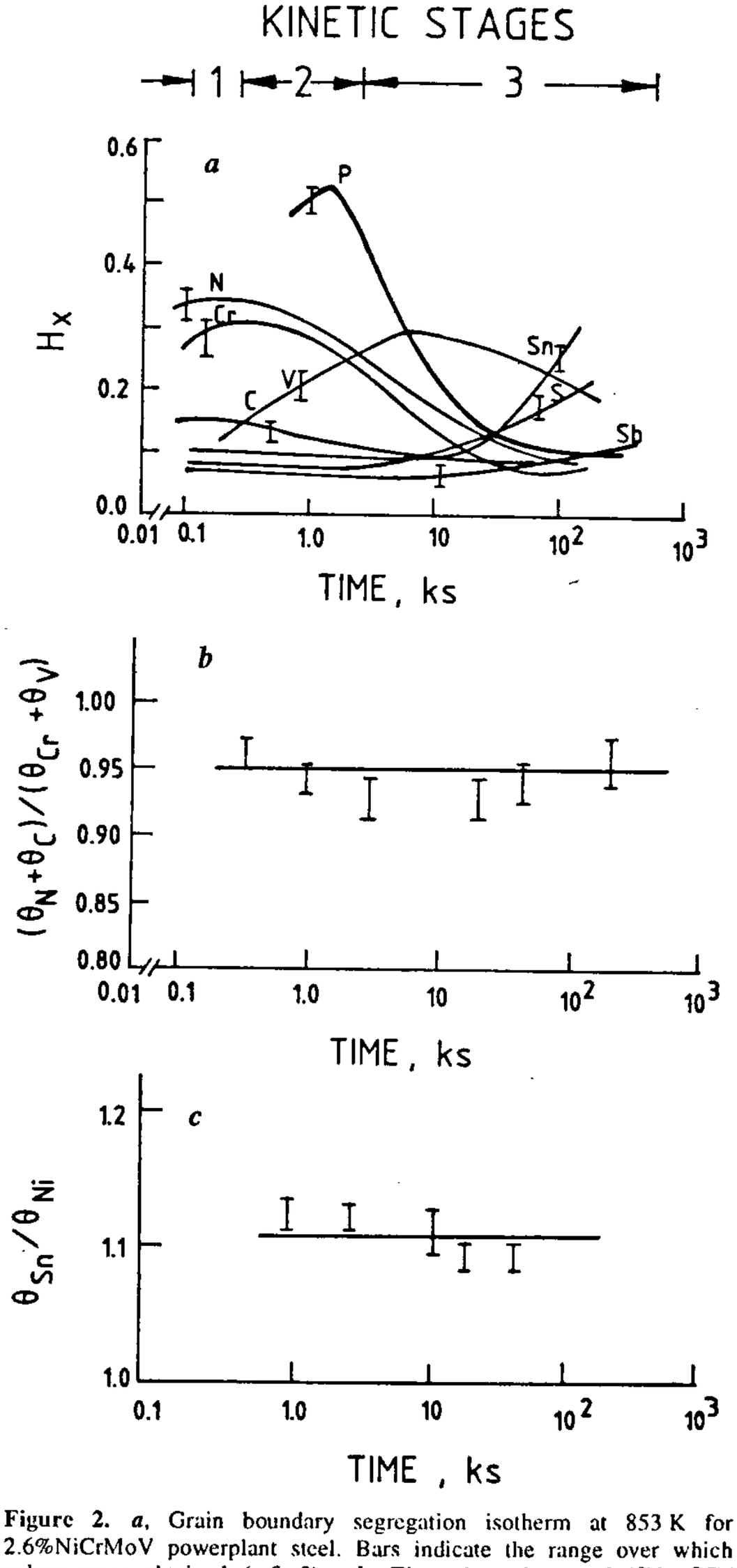

Figure 2. *a*, Grain boundary segregation isotherm at 853 K for 2.6%NiCrMoV powerplant steel. Bars indicate the range over which values were obtained (ref. 3). *b*, Time dependence of $(\theta N+\theta C)/(\theta Cr+\theta V)$, involving nitride and carbide forming-elements Cr and V, at 853 K (ref. 3). *c*, Time dependence of the ratio of coverages, $\theta Sn/\theta Ni$, for the cooperatively coupled elements Sn and Ni at 853 K (ref. 11).

by Edwards *et al.*[12] as the cause of embrittlement in a temper-embrittled steel.

Prolonged ageing at still higher temperature of 883 K brings about grain boundary site competition between Sn and S, with segregating S displacing segregated Sn (third kinetic stage; Table 2). This process is evident in Figure 3 *b* in terms of invariant $\theta_{Sn} + \theta_S$. This Sn–S interaction has implications to mechanical degradation processes such as creep cavitation[14].

With the help of data of the type described and discussed above, interaction maps can be drawn. The interaction maps, Figure 4 *a*, *b*, offer a perspective of the different interaction processes in time-temperature space. For example, the maps for the two Cr–Mo–V steels, with and without Ni, show that the presence of Ni does not make a difference to the Cr–N cooperative interaction (Figure 4 *c*). Ni–Sn coupling is seen only in the steel containing Ni. It is also easily inferred from the interaction maps that the S–Sn site competition occurs at higher temperatures, but after longer durations of exposure.

Table 2. Kinetic stages of isothermal grain boundary segregation of alloying and trace elements

Stage	Segregation behaviour
First stage	Cosegregation of Cr and N Desegregation of C
Second stage	Segregation of P (in association with V)
Third stage	Initially segregation of Ni and Sn and later desegregation of Ni and Sn accompanied by increase in S segregation

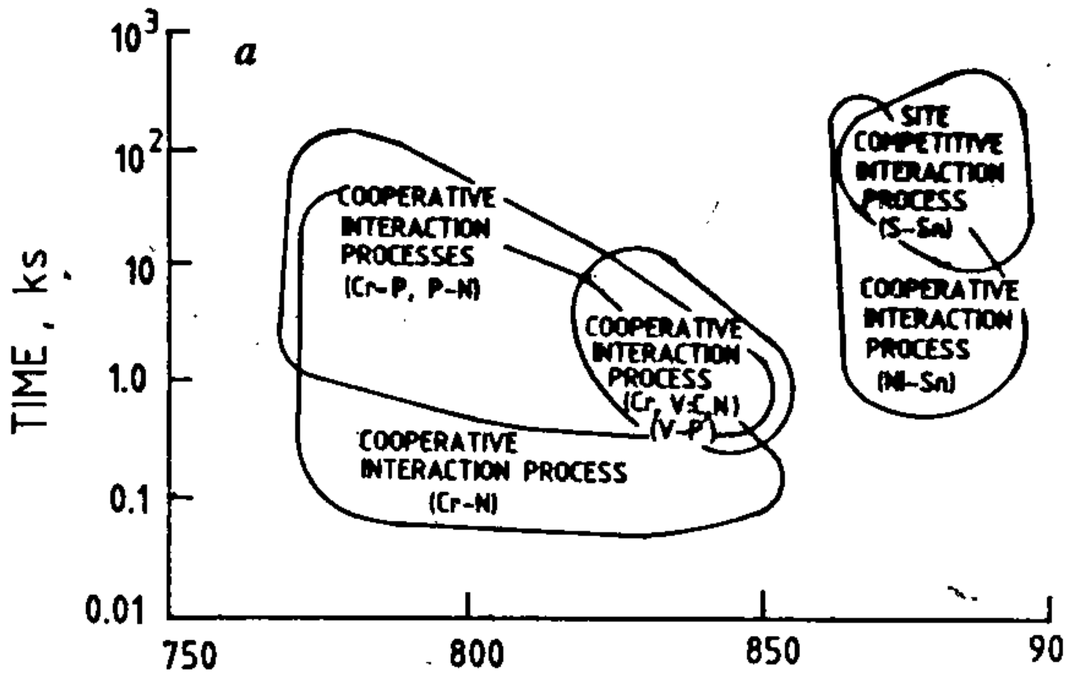

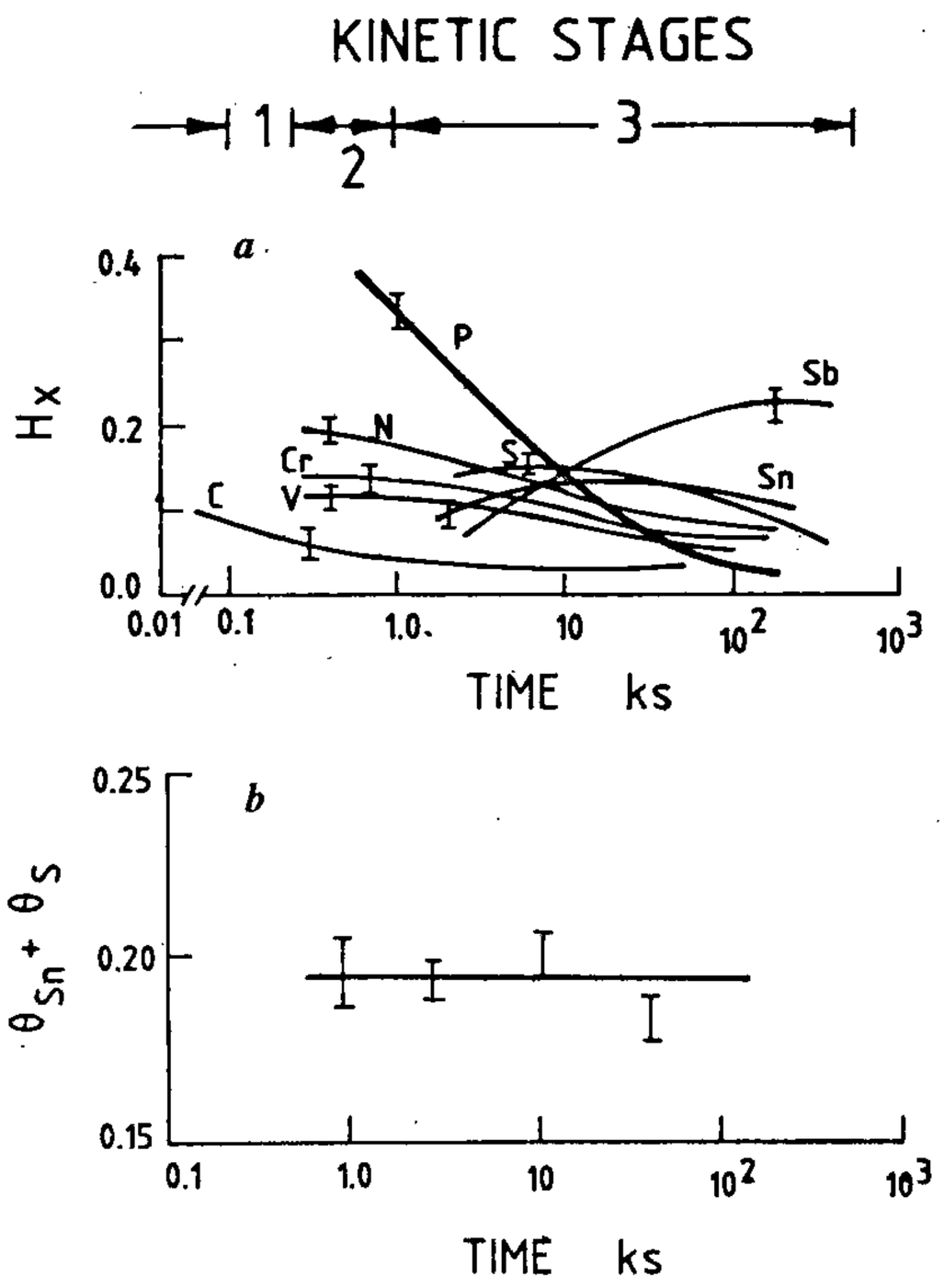

Figure 3. *a*, Grain boundary segregation isotherm at 883 K for 2.6%NiCrMoV powerplant steel. Bars indicate the range over which values were obtained (ref. 3). *b*, Time dependence of summation of the coverages, $\theta Sn + \theta S$, for the competitively interacting elements Sn and S at 883 K (ref. 11).

Figure 4. Interaction maps in time-temperature ($t - T$) space depicting grain boundary interactions occurring amongst trace and alloying elements in (*a*) 2.6%NiCrMoV, (*b*) 1.2CrMoV low alloy steels (ref. 4). (*c*) Interaction severity, ϕ, as a function of temperature for the cooperative Cr–N interaction process in 2.6%NiCrMoV and 1.2%CrMoV low alloy steels (refs 11, 31).

Isothermal grain boundary segregation data of solute and trace elements for the low Cr (solid lines) and high Cr (broken lines) steels at 773 K are presented in Figure 5 *a*, *b*. What Figure 5 presents is a remarkable finding[7]. While there is no difference in the segregation behaviour of N, Cr, S and Sn (Figure 5 *b*), the high Cr content in the steel leads to enhancement in the grain boundary concentration of P (Figure 5 *a*), also accelerates the rate of increase of grain boundary segregation of P (Table 3). The opposite trend is observed, i.e. lower C segregation, in the presence of higher Cr and more rapid desegregation. These observations, with regard to P and C, the only two elements markedly influenced by higher Cr, suggest a strong interdependency. There is confirmation here that the activity of C is reduced by the scavenging action of Cr which forms Cr-rich carbides and lowers C in solid solution. A natural consequence of lower dissolved C is lower extent of C segregation. The result of lower C segregation, which otherwise would have displaced P in a site-competitive process, is that grain boundary segregation of P is enhanced. Both these effects, i.e. increase of P (grain boundary embrittler) and lowering of C (grain boundary cohesion enhancer) contribute to a reduction in intergranular cohesion and an increase in susceptibility of the steel to intergranular embrittlement.

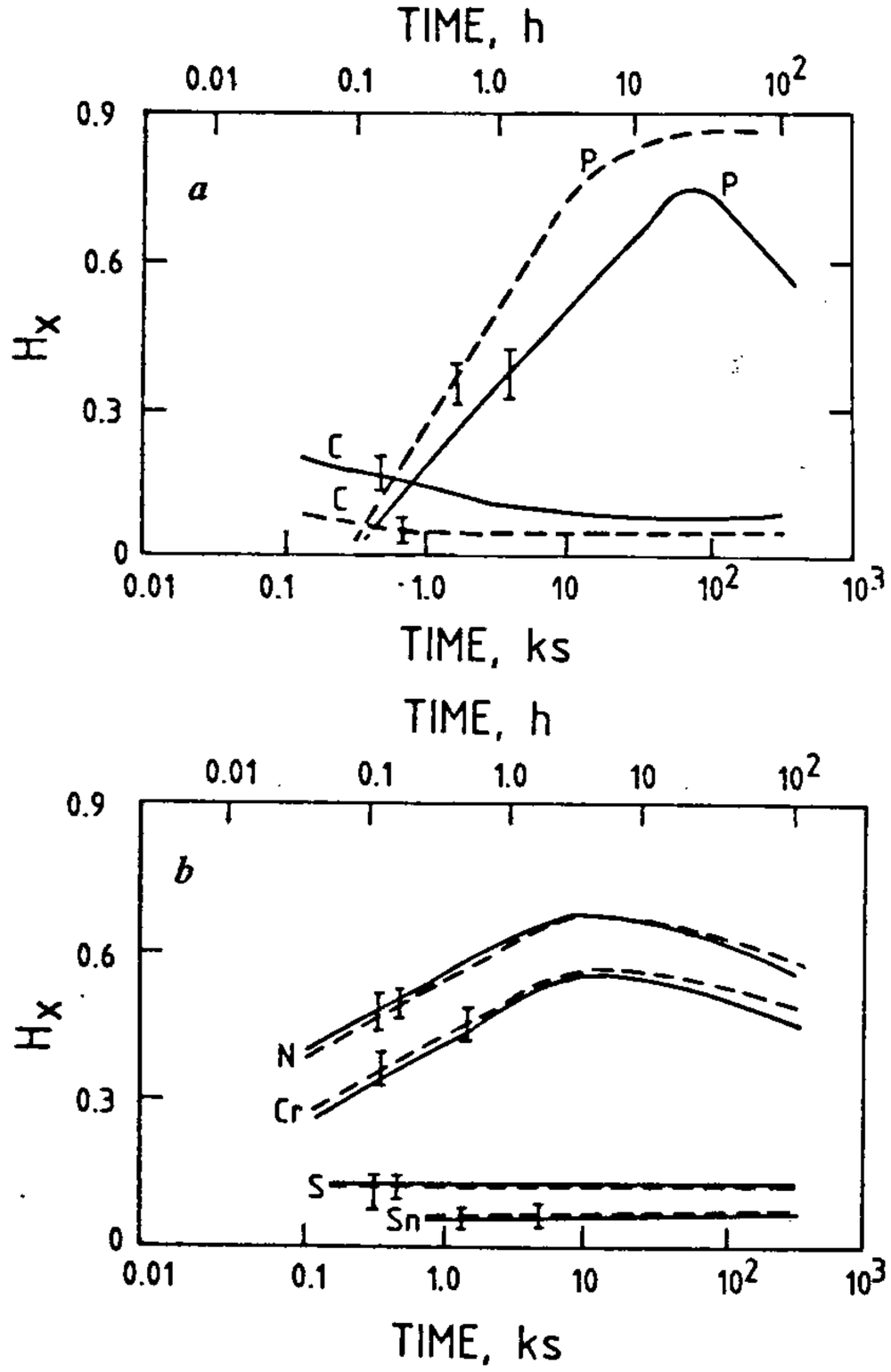

Figure 5. Grain boundary segregation isotherms recorded at 773 K for Fe-0.4Cr-2.6 Ni-0.28 Mo-0.1V (low chromium steel: solid lines) and Fe-11.27Cr-0.42Ni-0.42Mo-0.2V (high chromium steel: broken lines) steels. ***a***, elements affected by the presence of high chromium in steel, ***b***, elements not affected by the presence of high chromium in steel. Bars indicate the range over which values were measured (ref. 7).

Low alloy steels can be heat-treated to develop one of three commonly encountered microstructures (Figure 6). These are ferrite-pearlite, (Figure 6 *a*; slow cooling from high temperature austenite), bainite (Figure 6 *b*; cooled from austenite to intermediate temperature and held there before rapid cooling to room temperature) and (3) martensite (Figure 6 *c*; fast cooling from high temperature austenite).

The microstructural influence on the interaction severity (ϕ = ratio of coverage or summation of coverage for cooperative or site competitive interactions, respectively) is shown in Figure 7 for Cr–N (cooperative), Ni–Sn (cooperative) and Sn–S (site competitive) interactions which followed the sequence martensite > brainite > ferrite-pearlite[6]. The susceptibility to temper embrittlement increases in the same order[15] (Table 4).

Dynamic embrittlement

If, during the course of high temperature exposure, a tensile load is applied, significant enhancement in the grain boundary concentration of N, P and S and an acceleration in kinetics (Table 5) of their segregation ($\partial H_x/\partial \log t$) is observed[8]. Compare, for example, the segregation isotherms at 773 K shown for the unstressed Cr–Mo–V steel in Figure 1 *a* and those, at the same temperature, for the same steel in the stressed condition (Figure 8). Although the kinetic stages and the qualitative nature of the interactions were unaltered, the maximum in the grain boundary coverage of the elements was observed earlier. The activation energy for S diffusion, calculated from the isotherms data from the stressed material, was 106 kJ/mol which is close to the value[16] of grain boundary diffusion of S in α-Fe (119 kJ/mol) and about one-half of the reported[17] bulk diffusion activation energy in α-Fe (203 kJ/mol).

An attempt[18] has been made to differentiate the kinetics from the thermodynamic effects of the applied stress by determining grain boundary segregation isotherms

Table 3. Rate of segregation of C, N and P at 773 K (ref. 8)

Rate of segregation $\partial H_x/\partial \log t$	Low-Cr steel	High-Cr steel
$-\partial H_C/\partial \log t$	0.075	0.022
$\partial H_P/\partial \log t$	0.33	0.52
$\partial H_N/\partial \log t$	0.15	0.15

obtained from unstressed (Figure 9 *a*) and stress-aged specimens (Figure 9 *b*) in which an equilibrium coverage of grain boundary segregants had been reached prior to (Figure 9 *a*) stress-ageing. Figure 9 *b* shows that, on tensile loading, coverage of S increases during the first 3 h, or so, beyond which S decreases and attains the equilibrium concentration after about 20 h under load. These results[18] suggest that, in thermodynamic terms, because of development of a chemical potential gradient along two different grain boundary sites (Figure 10), S migrates from one grain boundary facet to the other via grain boundary diffusion (a process identified by activation energy measurements described above). On prolonged ageing, the stress-induced inhomogeneous distribution of S disappears as the slower diffusing species (host metal atoms) migrate to eliminate the transient sulphur concentration gradient. Thus, the transient enhancement of S concentration at the grain boundaries, as a result of stress application, and its subsequent reversal to its original equilibrium concentration are governed by mass-transport phenomena akin to those associated with diffusional creep under tensile loading[18].

The consequence of S ingress, under these circumstances, to high strength steels, subjected to loading at high temperatures, is diffusion controlled intergranular cracking, a phenomenon christened dynamic embrittlement[19–22]. Stress-driven diffusion of an impurity element causing intergranular decohesion has been observed by us in a Cu–Cr alloy[23]. The signature of dynamic embrittlement is crack-growth steps on the fracture surface, revealed as striations (Figure 11). The reason why growth steps occur is because, in this failure mode, we need a critical combination of stress and sulphur concentration to cause decohesion. The sequence during dynamic embrittlement[20] would be as follows: (i) Surfaces are contaminated by a mobile embrittling element (e.g. S in steel). (ii) Application of stress causes a rising

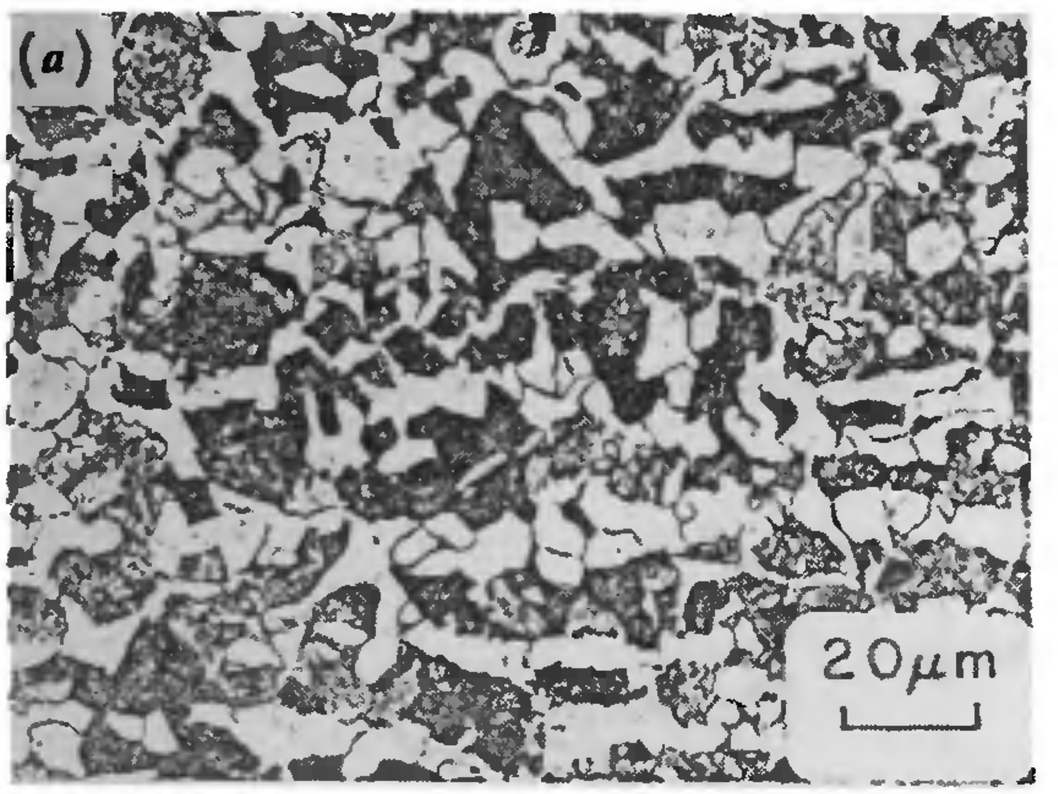

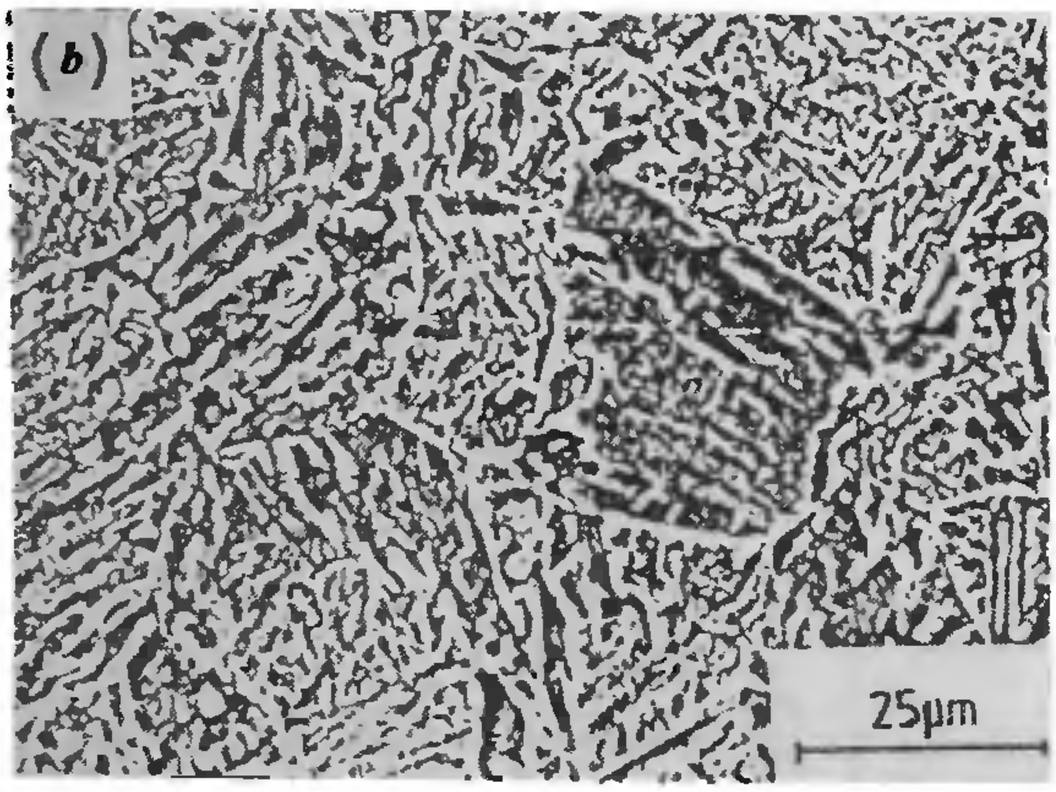

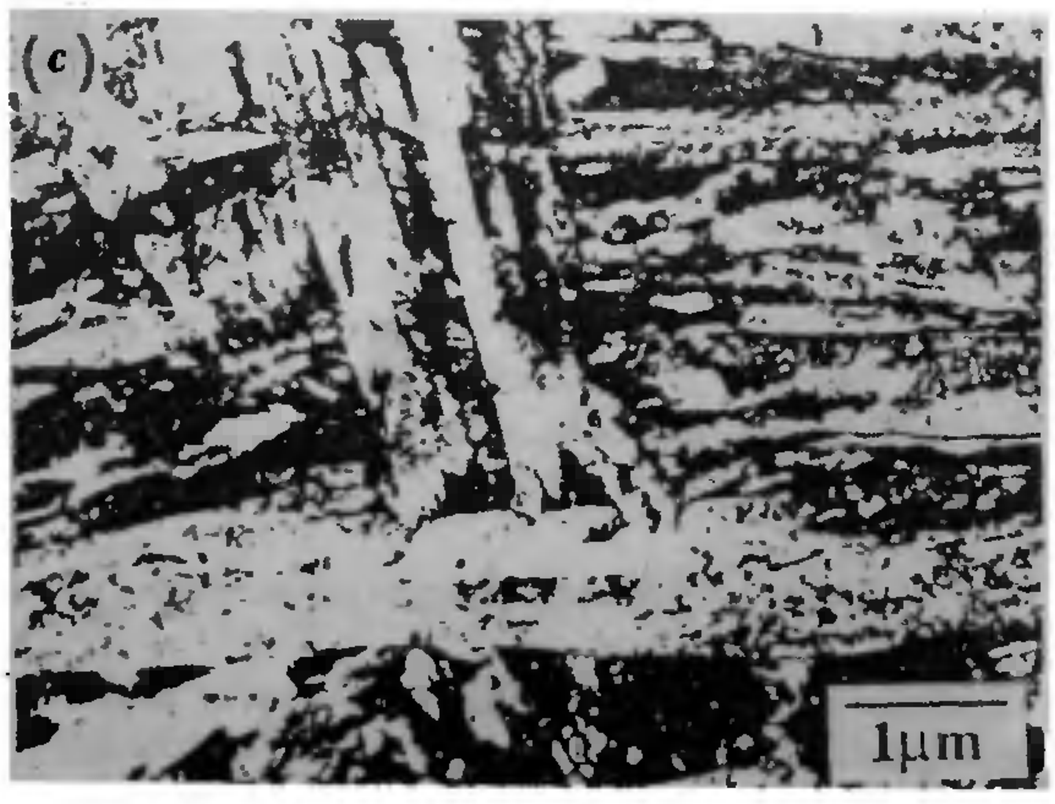

Figure 6. Microstructures encountered in steels: (*a*) ferrite-pearlite, (*b*) bainite and (*c*) martensite.

Table 4. Temper-embrittlement susceptibility as measured by the shift in ductile-to-brittle fracture appearance transition temperature (ΔFATT) (ref. 15)

Microstructure	ΔFATT, °C
Ferrite + pearlite	< 20
Bainite	25
Martensite	58

Table 5. Rate of segregation of N, P and S at different temperatures in Ni Cr Mo V power plant steel (ref. 5)

Temperature (K)	Kinetics of segregation $\partial H_x/\partial \log t$	Material condition	
		Unstressed	Stressed (353 MN/m²)
773	N	0.08	0.12
	P	0.24	0.28
	S	~0	0.02
823	N	0.079	0.126
	P	0.447	~1.0
	S	~0	0.063
853	N	0.215	0.274
	P	0.284	0.647
	S	0.0210	0.082

stress profile at the crack tip, providing a driving force for the diffusion of the element (S). The result is decohesion at a critical value of the combination of stress and S concentration and the crack advances (Figure 11). (iii) The process repeats. This stepwise crack growth is manifest as striations on the fracture surface revealed clearly in SEM picture (Figure 11). Dynamic embrittlement has been associated with such a common-place industrial process as stress-relief cracking of low-alloy steels[24,25] as well as low ductility intergranular fracture of as-quenched steels operated at elevated temperatures[26,27].

Rate of cooling

The rate of cooling, either after solution annealing or after ageing, that alloys containing trace elements are subject to, influences the degree of embrittlement. Step cooling methods have led to considerable embrittlement in metals. On the other hand, investigations have shown that embrittlement susceptibility is suppressed at cooling rates in excess of 50 K/h (ref. 11). Figure 12 shows that elemental segregation is strongly influenced by the applied cooling rate. A comparison of Figure 1 *a* with Figure 12 suggests that cooling from 773 K at 15 K/h alters the behaviour of grain boundary coverage of practically all the elements. The increase in grain boundary coverage is more marked in the case of P. This enhancement is a consequence of the decreasing solubility of P with decreasing temperature. Thus slow cooling, after solution annealing or ageing, can be potentially dangerous due to enhanced segregation of detrimental elements.

The precipitation hardened stainless steels, which are prone to grain boundary phosphorous embrittlement (to be discussed in the next section), are a typical instance in the context of a discussion of the cooling rate that the material is to be subjected to, after the ageing step in their heat treatment. Our studies[28] have shown that

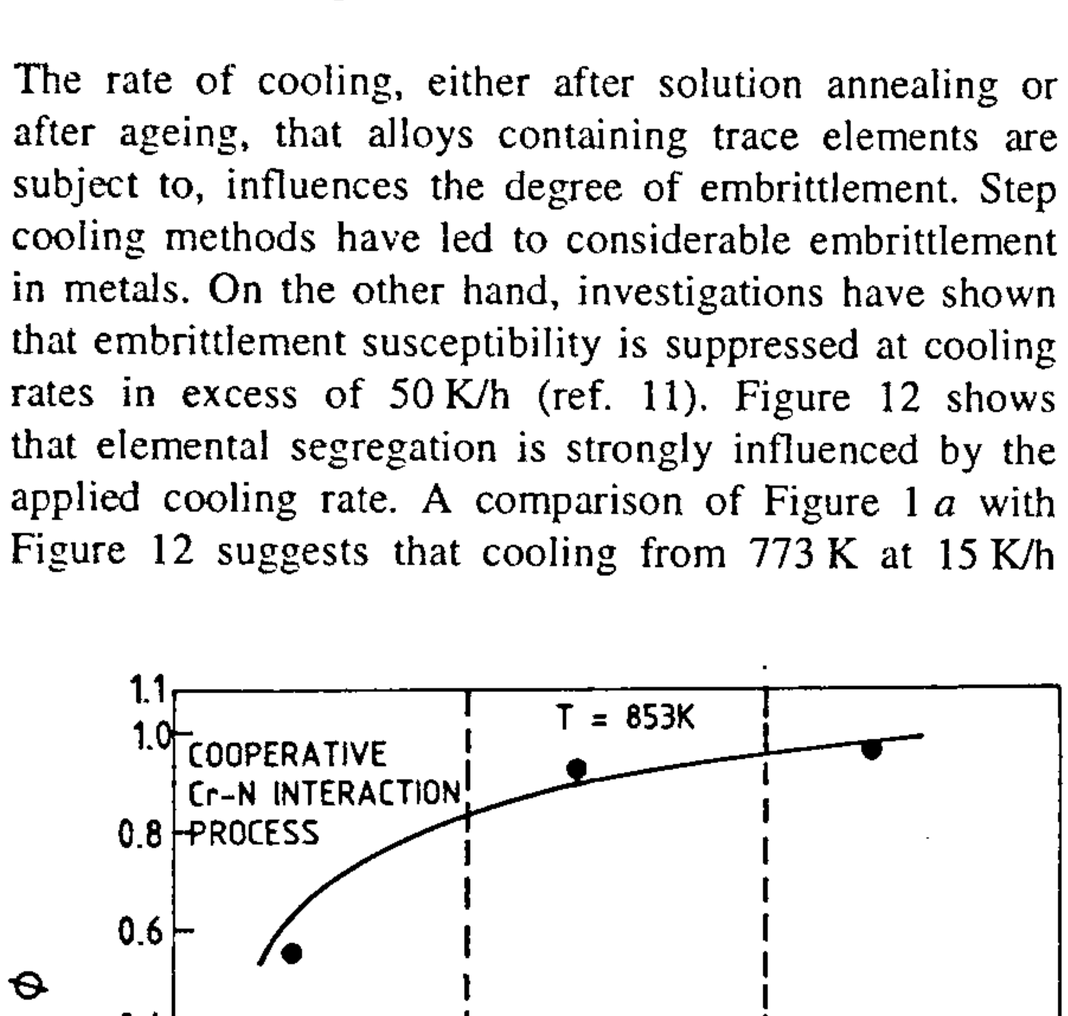

Figure 7. Interaction severity, ϕ, as a function of microstructure for the cooperative and site-competitive interaction processes in 2.6%NiCrMoV low alloy steel (ref. 11).

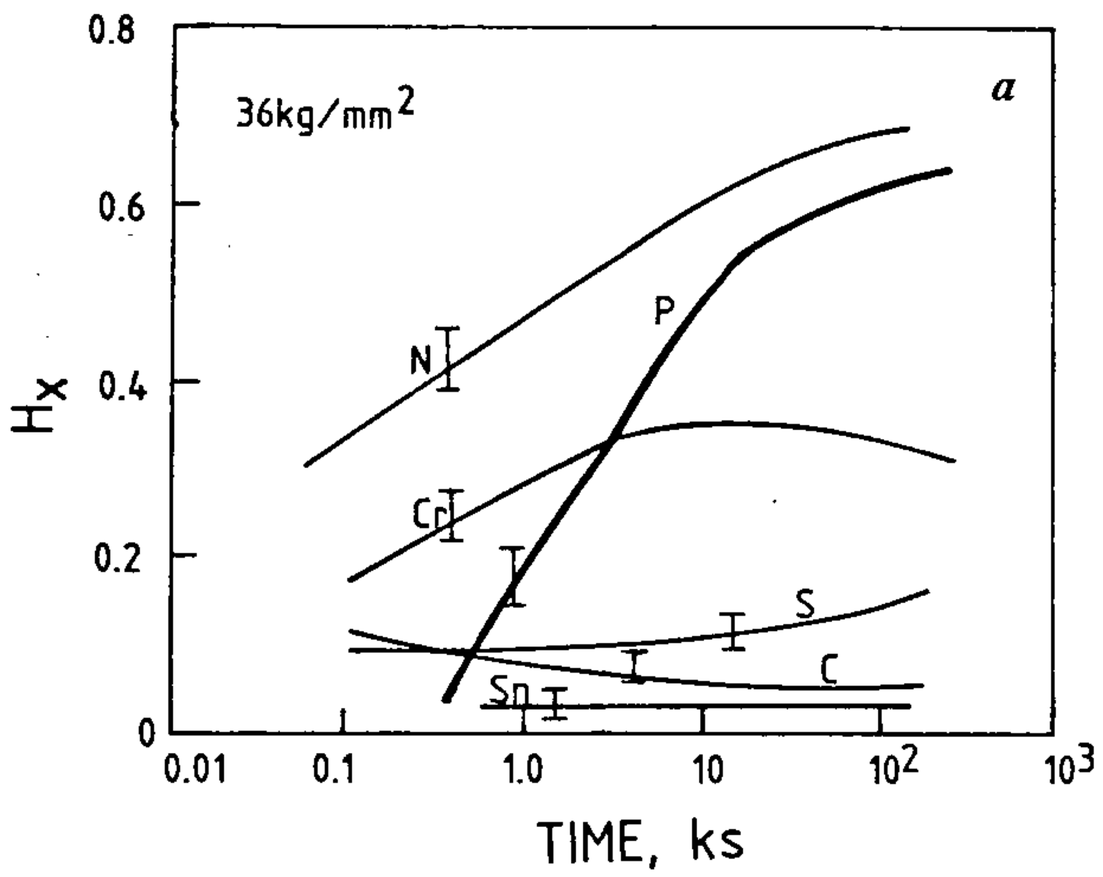

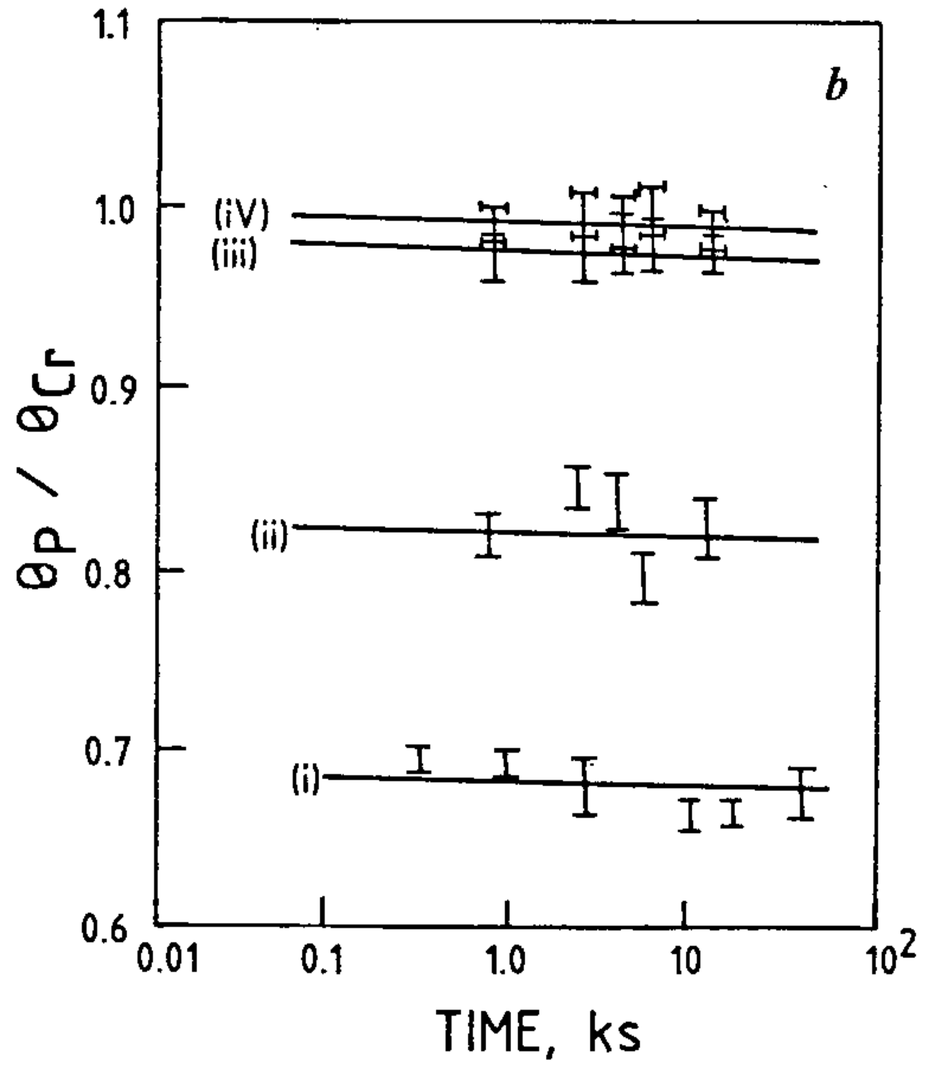

Figure 8. *a*, Segregation isotherm recorded at 773 K for low alloy steel stressed at 36 kg/mm^2 (ref. 8). *b*, θP/θCr as a function of time at 773 K for low alloy steel in: (i) Unstressed condition and stressed (ii) 36 kg/mm^2, (iii) 41 kg/mm^2 and (iv) 47 kg/mm^2 conditions (ref. 8).

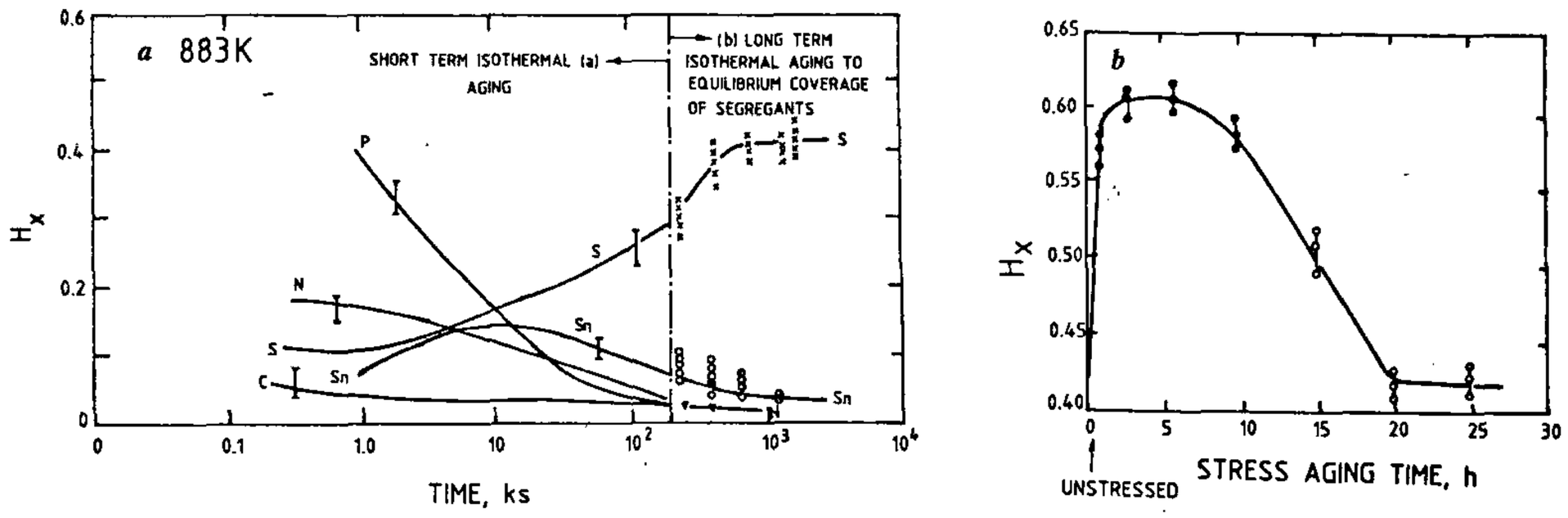

Figure 9. *a*, Grain boundary segregation isotherms recorded at 883 K on unstressed low 2.6%NiCrMoV alloy steel. Bars indicate the range over which values were observed (refs 11, 18). *b*, Grain boundary segregation isotherms recorded on the same steel in the stressed condition after prior ageing of specimens in the unstressed condition for 2160 ks at 883 K (ref. 18).

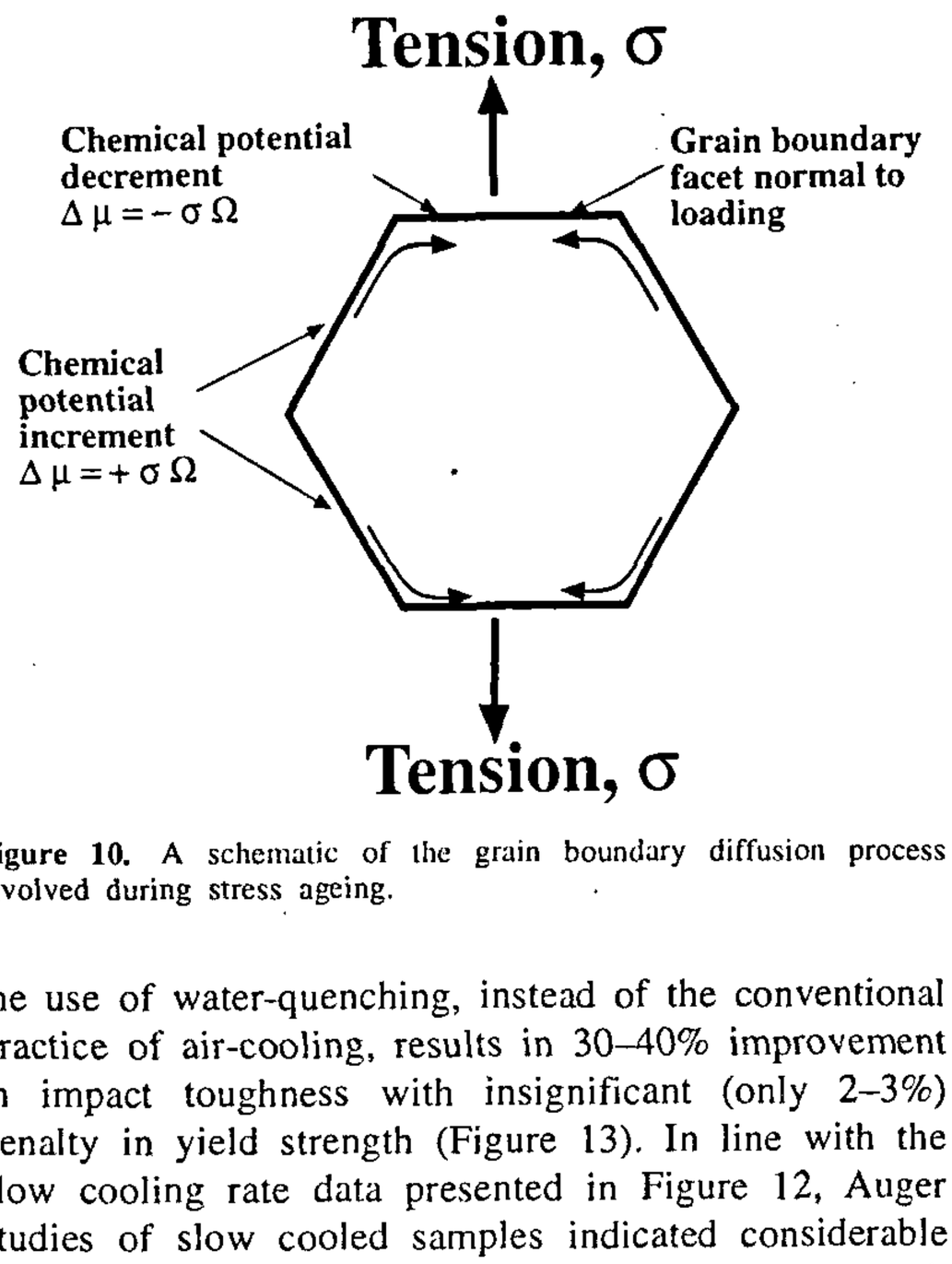

Figure 10. A schematic of the grain boundary diffusion process involved during stress ageing.

the use of water-quenching, instead of the conventional practice of air-cooling, results in 30–40% improvement in impact toughness with insignificant (only 2–3%) penalty in yield strength (Figure 13). In line with the slow cooling rate data presented in Figure 12, Auger studies of slow cooled samples indicated considerable grain boundary enhancement of P, whereas no such evidence of P was seen in the waterquenched samples.

Precipitation hardened stainless steels

The case of precipitation hardened stainless steels, produced at Midhani, Hyderabad, presents a notable example of the relevance of grain boundary segregation processes. These steels, which have the nominal composition (by wt.%) Fe-17Cr-4Ni-3Cu-0.4Mn-0.25Nb-0.2Si-0.02C-0.02 P-0.005S, are used in applications requiring superior mechanical properties combined with corrosion resistance. Midhani have supplied these steels to the Department of Atomic Energy for making nuclear power reactor components. During the course of their production, the steel was found to be prone to inconsistencies in impact toughness values in the products. There was heavy scatter in product impact toughness values from heat to heat, and from batch to batch for the same heat-treated condition. Although the tensile properties, namely yield strength, ultimate tensile strength and ductility parameters (per cent elongation and per cent reduction in area) were quite consistent and above the specified levels, the impact toughness values were found to scatter over a wide range from 5 to 120 Nm for fixed bulk content 0.28 wt% Nb.

Auger electron spectroscopy studies[29] conducted on samples from different heats indicated the presence of P at the grain boundaries. The grain boundary concentration of P was slightly on the lower side for the low C-content (~ 0.02%) melt in comparison with the melt with relatively higher C-content (0.035% C), which yielded in AES maximum segregation of P at the grain boundary. The impact toughness behaviour was opposite to that of the grain boundary concentration of P (Figure 14).

The strong dependence of impact toughness with bulk C-content was explainable in terms of Nb–C, Nb–P interactions. With the increase in bulk C-content, the grain boundary concentration of P would increase, because more and more Nb gets tied-up with C as NbC, and less is available to interact with P to form NbP. This would be so because the chemical interaction energy[30] for Nb–C interaction (~ 100–400 kcal/mol) is greater than that for Nb–P interaction (~ 30–50 kcal/mol). Phosphorous segregation was maximum at a C-concentration of 0.035%, corresponding approximately to the

value necessary to precipitate all of Nb (0.28%) as NbC with no Nb being available for interaction with P, or free dissolved C which could displace P from the grain boundaries. In melts with C-contents greater than 0.035%, the presence of free or excess C (Figure 14) displaces P effectively from the grain boundary, through C–P site-competitive process and, through resulting occupation, enhances grain boundary cohesion. Thus, at C-content greater than 0.035%, the grain boundary concentration of P is low.

Two distinct regimes are thus delineated (Figure 14): (a) a low toughness regime characterized by high grain boundary concentration of P and formation of Nb–C in the grain interior because of strong Nb–C interaction (Nb/C ratio > 6 but less than 20) and (b) a high toughness regime (Nb/C < 6), where grain boundary P is displaced by C through site-competitive process. The scatter in impact toughness values, as described above, was baffling as it occurred even though the chemical composition of the steel was as per specification in respect of each of the alloying elements. Once the Nb/C ratio was ensured to be less than 6, the product exhibited consistently high and acceptable impact values.

Thermodynamic analysis of grain boundary cohesion

A thermodynamic analysis in terms of free energy of segregation has been attempted[31] for the delineated low and high toughness regimes of Figure 14 following the approach of Rice and Wang[32] and Olson[33].

With reference to the first regime, which was characterized by low impact toughness and grain boundary segregation of P, the grain boundary segregation free energy of P can be obtained from[34]

$$\theta_P/(1-\theta_P) = X^B[P]\ \exp(-\Delta G_b^o[P]/RT), \qquad (1)$$

where θ_P is the grain boundary concentration of P, $X^B[P]$ is the bulk concentration of P, $\Delta G_b^o[P]$ is the segregation free energy of P, R is gas constant and T is the temperature in Kelvin.

The values of $\Delta G_b^o[P]$ obtained from equation (1) for regime I, after substitution of appropriate values from Figure 15 *b*, are presented in Figure 15 *c*. The experimentally calculated values are in the range 38–49 kJ/mol.

With reference to regime II, which is characterized by grain boundary displacement of P by carbon (site-competitive process), equation (1), can be written as:

$$\theta_P = X^B[P]\ (1-\theta_P-\theta_C)\ \exp(-\Delta G_b^o[P]/RT), \qquad (2)$$

$$\theta_C = X^B[C]\ (1-\theta_P-\theta_C)\ \exp(-\Delta G_b^o[C]/RT), \qquad (3)$$

where θ_C is the grain boundary concentration of P; $X^B[C]$ is the bulk concentration of C; $\Delta G_b^o[C]$ is the grain boundary segregation free energy of C. In equations (2) and (3), it is assumed that there is no energetic interaction between C and P. The values of $\Delta G_b^o[P]$ and $\Delta G_b^o[C]$ obtained for regime II, after substituting the values of $X^B[P]$ and $X^B[C]$, θ_P, θ_C for each of the compositions (heats) presented in Figure 15 were in the range 33–42 kJ/mol and 60–72 kJ/mol, respectively. The values of $\Delta G_b^o[P]$ and $\Delta G_b^o[C]$ were in the scatter band

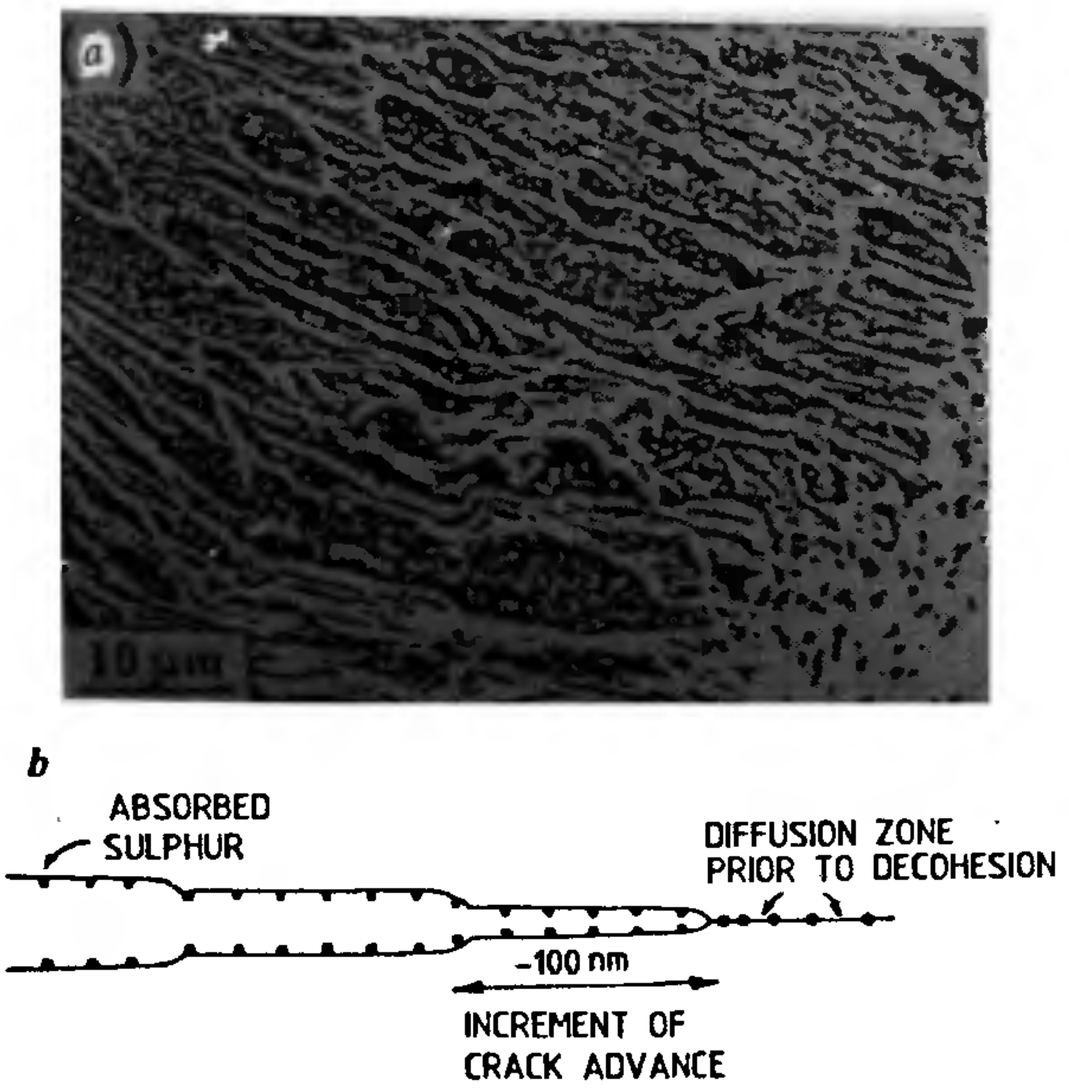

Figure 11. *a*, An intergranular fracture surface of Cu–Cr alloy showing striations with line-up of voids containing Cr-particles (ref. 23). The presence of striations in the intergranular region is consistent with quasi-static, step-wise crack growth expected in dynamic embrittlement (*b*) (ref. 20).

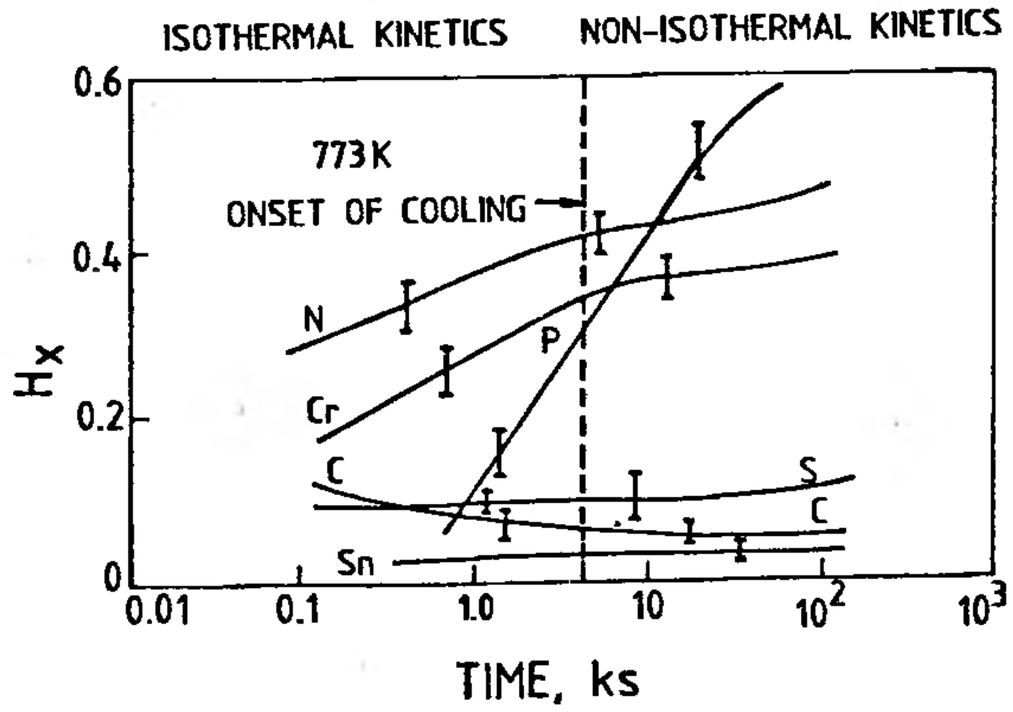

Figure 12. Isothermal and non-isothermal kinetic plots for 2.6%NiCrMoV steel soaked at 773 K and subsequently cooled at the rate of 15 K/h. The onset of cooling is indicated by the broken line (ref. 11).

of ± 10 kJ/mol and are only marginally lower than the reported mean values of $\Delta G_b^o[P] = 50$ kJ/mol and $\Delta G_b^o[C] = 80$ kJ/mol (ref. 34) obtained for much simpler systems.

Rice and Wang[32] have presented a thermodynamic framework for treating the embrittlement of interfaces by solute segregation in terms of the ideal work of interfacial separation, $2\gamma_{int}$. Their hypothesis suggests that the control of $2\gamma_{int}$ is the most effective means of enhancing interfacial fracture resistance and that the embrittlement (or ductilization) by impurity solute segregation can be explained in terms of the effect of segregation on $2\gamma_{int}$, such that[32]:

$$2\gamma_{int} = (2\gamma_{int})_o - (\Delta G_b^o - \Delta G_s^o)\tau, \quad (4)$$

where $(2\gamma_{int})_o$ is the work of separation of the clean interface, τ is the excess interfacial solute coverage (concentration of segregant per unit area at the interface), and ΔG_b^o–ΔG_s^o are the free energies of segregation of the solute to the boundary and the free surface respectively, evaluated at the temperature of fracture, (taken as 300 K). Equation (4) predicts that a segregating solute with a greater (more negative) segregation energy at a free surface compared to an internal boundary will embrittle (reduced $2\gamma_{int}$), while one with a lower energy at a boundary compared to the free surface will enhance interfacial cohesion (increased $2\gamma_{int}$)[32,33]. The results of fracture experiments which can enable the determination of the change in $2\gamma_{int}$ as a consequence of solute segregation are not available. However, the effects of segregants are available in terms of their effect on the ductile–brittle transition temperature (DBTT). The effects of embrittling elements have generally been reported as variations δ(DBTT) in DBTT associated with variation in solute coverage, $\delta\tau$ and correlated as:

$$\delta(\mathrm{DBTT}) = \Sigma E\, \delta\tau, \quad (5)$$

where E is the embrittlement sensitivity in Kelvin/atomic% of solute at the grain boundary. The best measure of embrittling sensitivity available is the shift of intergranular ductile–brittle transition temperature per amount of segregated solute. According to the hypothesis of Rice and Wang[32] solute segregation influences DBTT through its effect on $2\gamma_{int}$. Thus from the above discussion:

$$(\delta\mathrm{DBTT}/\delta\tau) \propto (\Delta G_b^o - \Delta G_s^o). \quad (6)$$

Since DBTT values for different industrial heats of this 17–4 PH stainless steel containing varying carbon content were not available, DBTT was considered to be inversely related to the impact toughness and a plot was attempted of the inverse of the product of impact toughness and atomic% segregant (considered to represent embrittlement sensitivity and denoted as E) as a function of ΔG_b^o–ΔG_s^o (Figure 16). The value of $-\Delta G_s^o$(76–80 kJ/mol) taken for determination of ΔG_b^o–ΔG_s^o corresponds to AES-based surface segregation data in polycrystalline iron[35]. The range of the observed values of E, and the corresponding range ΔG_b^o–ΔG_s^o, for each of the heats is depicted in the form of a box by a solid line, followed

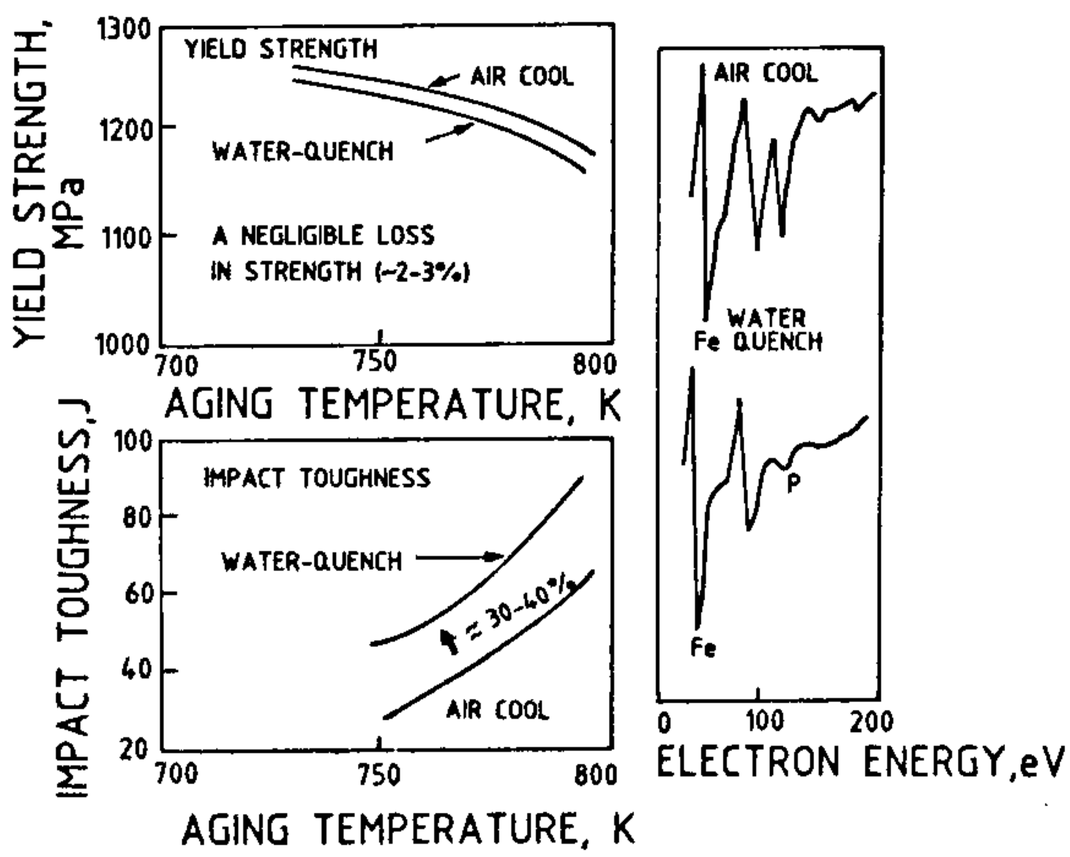

Figure 13. Influence of post ageing quenching treatment on impact toughness of 17Cr-4Ni precipitation hardened stainless steel (refs 11, 28).

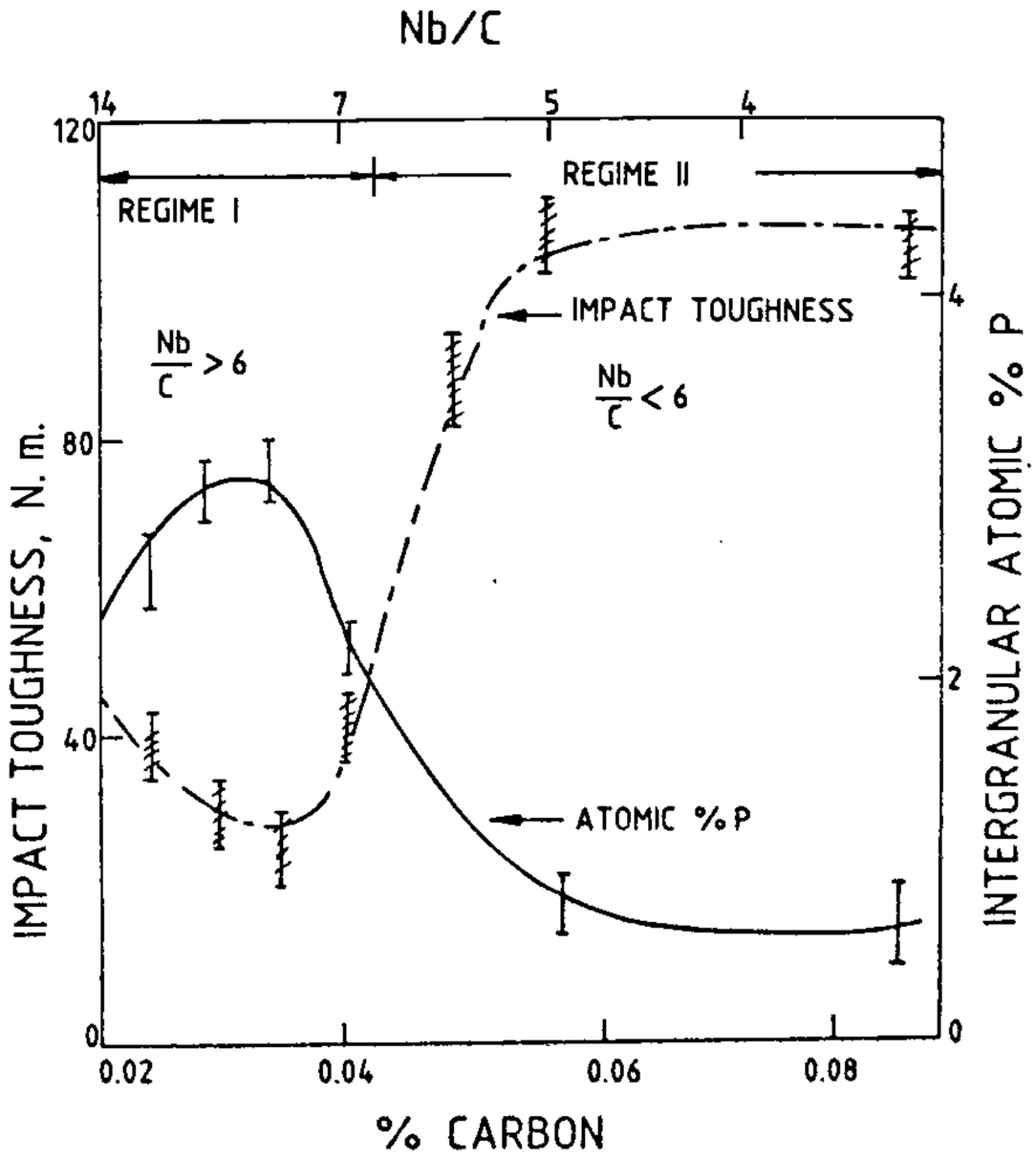

Figure 14. Variation of impact toughness and intergranular atomic% P with % C in 17-4 PH stainless steel (ref. 29).

by summarization with broken lines. Figure 16 predicts, as in the work of Olson[33], that P, an element with more positive $\Delta G_b^\circ - \Delta G_s^\circ$, is more embrittling as compared to C with less positive $\Delta G_b^\circ - \Delta G_s^\circ$ and supports the results presented[31] in Figure 15. The approach of using $\Delta G_b^\circ - \Delta G_s^\circ$, as one of the parameters, for understanding intergranular embrittlement and its control at the electronic level is being further advanced and we will describe this aspect briefly in the last section.

Thermodynamic and electronic basis of embrittlement

There are a number of issues pertaining to the phenomena and the results described above that require explanation on a more fundamental basis. In this respect, important contributions have been made by Rice[32] and Olson[33]. It is instructive to briefly describe their approaches.

The problem that is to be addressed is the commonly observed phenomenon that iron is embrittled by grain boundary segregation of P and S, as also trace impurities of elements belonging to groups IV and V (tin, antimony and arsenic). On the other hand, a small amount of dissolved C alleviates the situation. The explanation is that C experiences a strong attraction to the grain boundaries which, when happens, displaces embrittling impurities such as P from the grain boundaries (e.g. the case of 17–4 PH stainless steel discussed above). There is evidence[1] to suggest that carbon increases the cohesive strength of iron grain boundaries. This seems to be true also of two other interstitials, B and N, as experimental observations indicate with respect to their behaviour in transition metals and alloys (e.g. the celebrated discovery[36] of trace B ductilizing brittle intermetallic Ni_3Al which has made possible industrial products out of Ni_3Al). The covalent radii of these interstitials are larger than their lattice sites. The driving force for their segregation is provided by the release of elastic energy

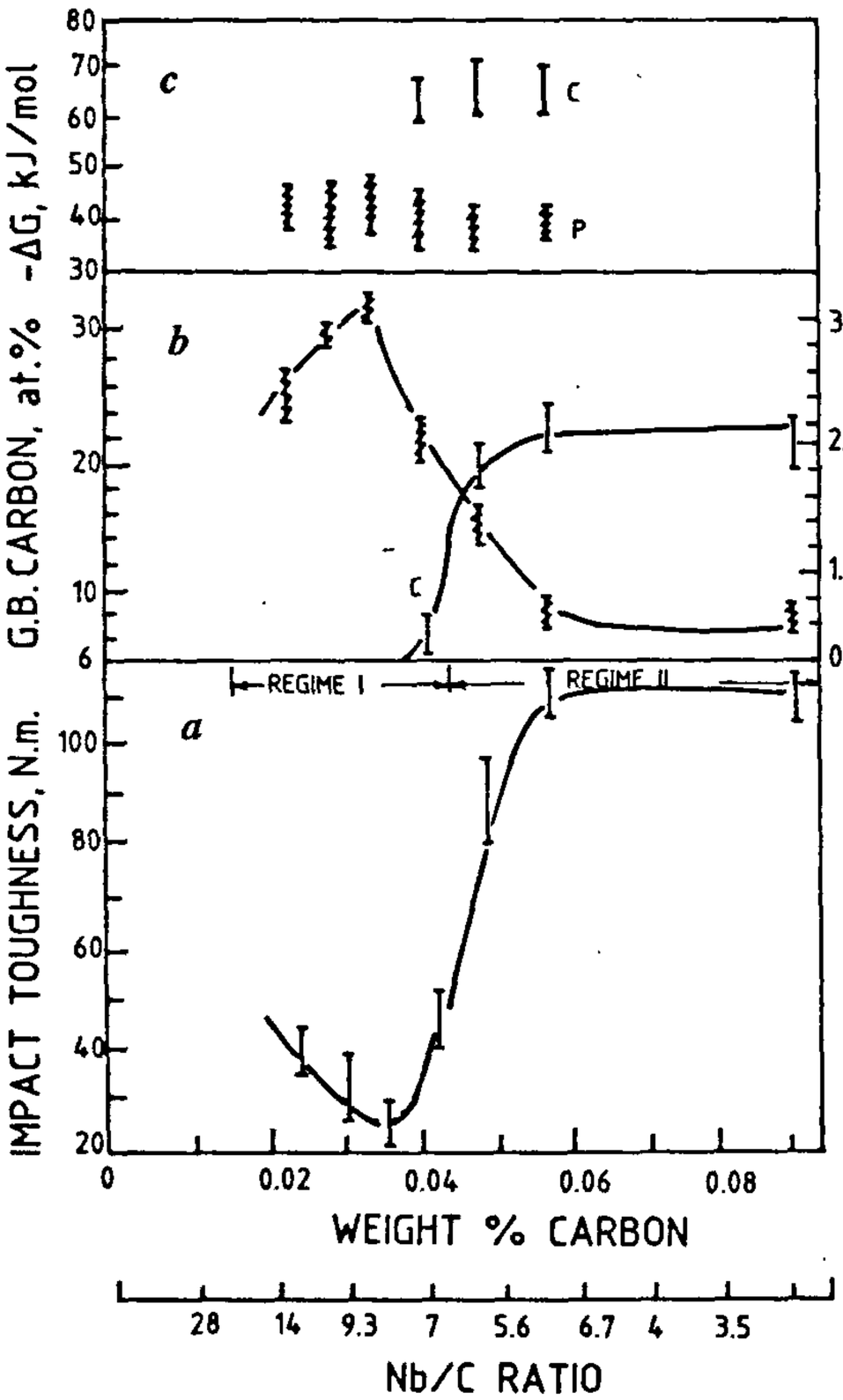

Figure 15. Impact toughness (*a*), intergranular atomic% C and P (*b*), and ΔG°[P] and ΔG°[C], (*c*) as a function of bulk wt% C (also Nb/C ratio) in 17Cr–4Ni pH stainless steel (ref. 11).

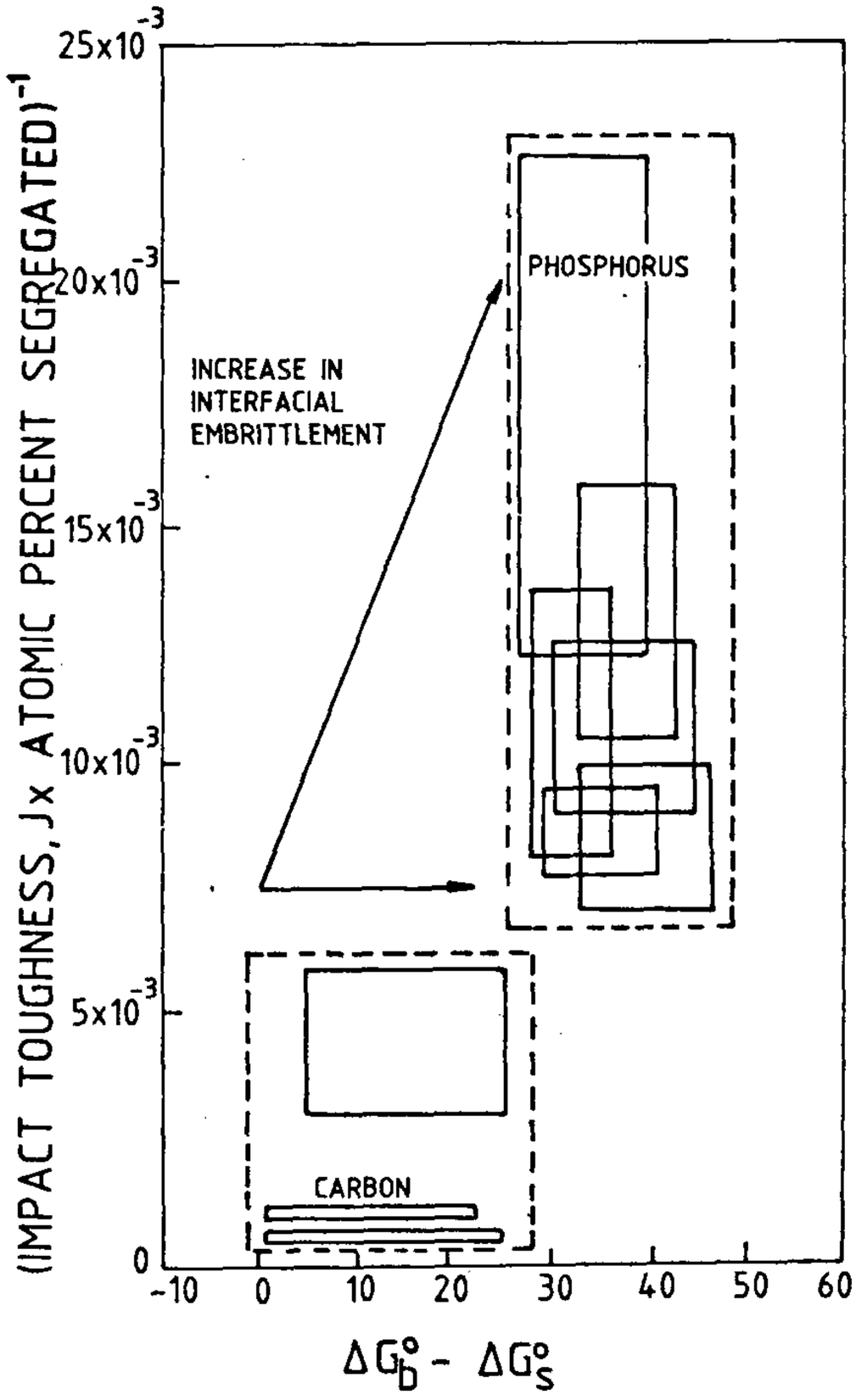

Figure 16. Inverse of the product of impact toughness and atomic% segregant (C or P) as a function of $\Delta G_b^\circ - \Delta G_s^\circ$ in 17Cr–4Ni PH stainless steel (ref. 31).

when the interstitials migrate to the larger spaces available at incoherent, large angle grain boundaries[37]. The driving force is also attributable to the large Pauli repulsion energy of the electrons of these atoms in sites of high host electron density such as unrelaxed interstitial sites in the transition metals[37]. The aim here is to understand the interactive effects observed in the segregation behaviour (e.g. as noted in the work on segregation isotherms). The question, however, which remains to be answered is that why does P act as a grain boundary embrittler while C or B perform as enhancers of grain boundary cohesion?

Before dealing with the above question, reference must be made to the work of Dumoulin and Guttman[38] who have studied, from a thermodynamic perspective, the segregation of metallic additions to iron (Ni, Cr, Mo and so on) and metalloid impurities (P, Sb, C, S, N and so on). Quantitative measurements were made of equilibrium segregation of the metal and the metalloid elements as a function of temperature. Using these measurements, the published thermodynamic and solid solubility data, solid state physics properties that reflect the propensity to short or long range order, Dumoulin and Guttman[38] have assessed and classified interaction coefficients at the free surface between the metal and the metalloid elements playing a role in grain boundary embrittlement and compared them with the corresponding values at the grain boundaries and with bulk values. This work broadly rationalizes the observed segregation behaviour of the metal and the metalloid elements and the interaction processes among trace and alloying elements.

Returning to the question of the action of P or C at the grain boundary site, the principle is contained in the equation (4) used in the previous section. The principle[32] is that $2\gamma_{int}$ can be regarded as the controlling interfacial property. $2\gamma_{int}$, the work of separation of clean interface, is the ideal work of separating an interface against atomic cohesion and is given by (Figure 17) the area under the plot of stress σ versus separation distance X. The competition between brittle interfacial cleavage separation and crack tip blunting by dislocation emission governs the observed brittle or ductile behaviour.

Brittle fracture occurs when

$$G_{disl} > 2\gamma_{int}$$

and ductile failure prevails when

$$G_{disl} < 2\gamma_{int},$$

where G_{disl} is the critical crack extension force (or strain energy release rate) for crack tip dislocation emission. This is the basis of the equation (4).

The experimental and available thermodynamic data for Fe grain boundary and free surfaces with impurities such as P, C, B, Sn, Sb, S support the relationship expressed in equation 4.

The value of $\Delta G_b^o - \Delta G_s^o$ is related to the interatomic chemical bonding and can be determined by using the state-of-art quantum mechanical calculations. Olson *et al.*[39] have carried out full potential linearized augmented plane wave (FLAPW) total energy calculation using a slab model for the grain boundary as well as free surface to investigate the effect on cohesion of a segregant like P or B (effect of B analogous to that of C) impurity in the boundary and the corresponding free surface. $\Sigma 3$ [1$\bar{1}$0] (111) grain boundary is studied for this purpose. ($\Sigma 3$ refers to a spatial orientation relation between crystals for which one in 3 lattice points is coincident), [1$\bar{1}$0] to crystal indices of the axis of misorientation and (111) to the habit plane of the boundary). The authors obtained equilibrium geometries from DMOL cluster force calculations. The calculated binding energies are composed of (a) mechanical energy component arising from structural relaxation associated with the presence of the impurity, a chemical component and a magnetic contribution. P is a larger atom (1.09 Å) compared to B (0.97 Å) but the mechanical energy difference is not very significant. P has three 3p electrons ($1S^2 2S^2 2p^6 3S^2 3p^3$) while B has one 2p electron ($1S^2 2S^2 2p^1$) with the result that the lone 2p electron in B occupies the p_{xy} state leaving the p_z state empty; the p state hybridizes with the neighbour Fe d_z state causing charge transfer from the in-plane p_{xy} state to the vertical pz state[39]. Thus B–Fe bonding shows stronger spatial anisotropy. B effects on magnetization of the surrounding atoms is weaker but it turns out that, for B at free surface, (ΔG_s^o), the reduction in chemical energy component is much greater (one out of two B–Fe bonds is broken in free surface while three out of five bonds are broken for P). Therefore the chemical part of $\Delta G_b^o - \Delta G_s^o$ for B in equation 4 is nearly twice as large as that for P (ref. 39).

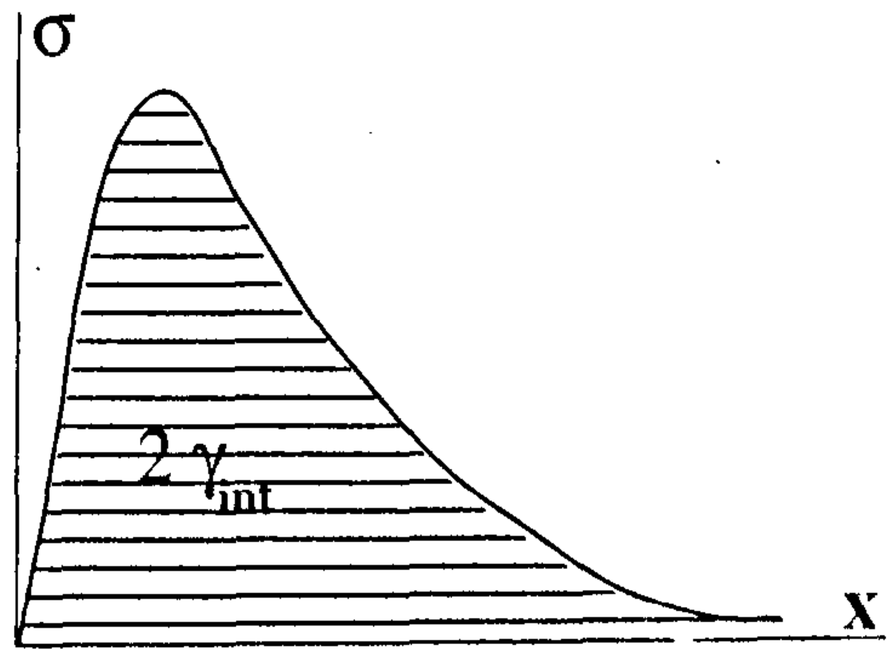

Figure 17. A schematic of stress versus separation distance normal to an interface.

Concluding remarks

The discussion points to a grand manner of coming together of the mechanics engineer, the materials scientist and the quantum physicist and the effectiveness of thermodynamics as a medium of communication across disciplines. The design of steels for specific property development has traversed a long path. The journey has not ended despite the advent of ultra high strength steels (with yield strengths of about 2000 MPa) and ultra high fracture toughness (in excess of 100 MPa$\sqrt{m}$). There is the issue of stress corrosion cracking resistance, typically a grain boundary property. The understanding of the type that has emerged hopefully will result in *ab-initio* successful design approaches to design against stress corrosion cracking failure at high strength levels.

1. Rama Rao, P., *Curr. Sci.*, 1996, **70**, 358–372.
2. Seah, M. P., in *Practical Surface Analysis* (eds Briggs, D. and Seah, M. P.), Wiley, London, 1983, pp. 181, 311–356.
3. Misra, R. D. K., Balasubramanian, T. V. and Rama Rao, P., *Acta Metall.*, 1987, **35**, 2995–3000.
4. Misra, R. D. K. and Balasubramanian, T. V., *Acta Metall.*, 1989, **37**, 1475–1483.
5. Misra, R. D. K. and Balasubramanian, T. V., *Acta Metall.*, 1990, **38**, 1263–1266.
6. Misra, R. D. K. and Balasubramanian, T. V., *Acta Metall.*, 1990, **38**, 2357–2366.
7. Misra, R. D. K. and Rama Rao, P., *Acta Metall.*, 1991, **39**, 2183–2187.
8. Misra, R. D. K. and Rama Rao, P., *Acta Metall.*, 1992, **40**, 1223–1228.
9. Misra, R. D. K. and Rama Rao, P., *Mater. Sci. Tech.*, 1993, **9**, 497–501.
10. Misra, R. D. K., *Scr. Metall. Mater.*, 1991, **25**, 1109–1110.
11. Misra, R. D. K. and Rama Rao, P., *Mater. Sci. Tech.*, 1997, **13**, 277–288.
12. Edwards, B. C., Eyre, B. L. and Crankshaw, T. E., *Nature*, 1977, **269**, 47–48.
13. Guttmann, M., *Sur. Sci.*, 1975, **53**, 213–227.
14. Yu, J. and Grabke, H. G., *Met. Sci.*, 1983, **17**, 389.
15. Viswanathan, R., in *Optimisation of Processing, Properties and Service Performance through Microstructural Control* (eds Abrams, H., Maniar, G. N., Nail, D. A. and Solmon, H. D.), ASTM STP 672, 1979, pp. 169–185.
16. Carbonnaux, C., Dessieux, C. R., Cizeron, G., Larera, A., Nguyen, T. T., Saindrenan, G. and Roptin, D., *Colloq. Phys.*, 1990, **C151**, 789.
17. Oikawa, O., *Technol. Rep. Tohoku Univ.*, 1992, vol. 48, p. 7.
18. Misra, R. D. K., *Acta Metall. Mater.*, 1996, **44**, 895–890.
19. Bika, D. and Mc Mahon, C. J., *Mater. Res. Soc. Symp. Proc.*, 1992, **238**, 339.
20. Bika, D., Pfaendtener, J., Menyhard, M. and McMahon, C. J., *Acta Metall. Mater.*, 1995, **43**, 1895–1908.
21. Bika, D. and McMahon, C. J., *Acta Metall. Mater.*, 1995, **43**, 1909–1916.
22. Misra, R. D. K., McMahon, C. J., Jr. and Guha, A., *Scr. Metall. Mater.*, 1994, **31**, 1471–1474.
23. Misra, R. D. K., Satya Prasad, V. and Rama Rao, P., *Scr. Metall. Mater.*, 1996, **35**, 129–133.
24. Shin, J. and McMahon, C. J., *Acta Metall.*, 1984, **32**, 1534–1552.
25. Shin, J. and McMahon, C. J., *Met. Sci.*, 1984, **18**, 403.
26. Hippsley, C. A., Knott, J. F. and Edwards, B. C., *Acta Metall.*, 1982, **30**, 641–654.
27. Lewandowski, J., Hippsley, C. A. and Knott, J. F., *Acta Metall.*, 1987, **35**, 2081–2090.
28. Misra, R. D. K., Prasad, C. Y., Balasubramanian, T. V. and Rama Rao, P., *Scr. Metall.*, 1988, **22**, 1323–1325.
29. Misra, R. D. K., Prasad, C. Y., Balasubramanian, T. V. and Rama Rao, P., *Scr. Metall.*, 1986, **20**, 713–716; 1339–1342.
30. Ustinovshchikov, J. I., *Acta Metall.*, 1983, **31**, 355–364.
31. Misra, R. D. K. and Rama Rao, P., *Scr. Metall. Mater.*, 1993, **28**, 153–156.
32. Rice, J. R. and Wang, J. S., *Mater. Sci. Eng.*, 1989, **A107**, 23–40.
33. Olson, G. B., in *Innovations in Ultrahigh Strength Steel Technology* (eds Olson, G. B., Azrin, M. and Wright, E. S.), Proceedings of the 34th Sagamore Army Materials Research Conference, August 30 to September 3, 1987, Lake George, New York, 1990, pp. 3–66.
34. Erhart, H. and Grabke, H. J., *Met. Sci.*, 1981, **15**, 401–408.
35. Guttmann, M., in *Atomistics in Fracture* (eds Latanision, R. M. and Pickering, J. R.), Plenum Press, New York, 1983, pp. 465–494.
36. Aoki, K. and Izumi, O., *J. Japan Inst. Met.*, 1979, **43**, 1190.
37. Cottrell, A. H., *Mater. Sci. Tech.*, 1991, **7**, 585–586.
38. Dumoulin, P. and Guttmann, M., *Mater. Sci. Eng.*, 1980, **42**, 249–263.
39. Ruqian, Wu., Freeman, A. J. and Olson, G. B., *Science*, 1994, **265**, 376–380.

ACKNOWLEDGEMENTS. Dr R. D. K. Misra spearheaded the work on Auger electron microscopy studies of grain boundary segregation with exemplary dedication at the Defence Metallurgical Research Laboratory. He was ably supported by Mr T. V. Balasubramanian. My presentation was made possible by their work. Grateful thanks are due to Shri S. L. N. Acharyulu, Director, Defence Metallurgical Research Laboratory for his unstinted help and several colleagues for their cooperation. I must also express grateful appreciation of the contributions made by colleagues at Mishra Dhatu Nigam Limited in the work described on 17–4 PH stainless steel.

Received 13 September 1997; accepted 16 September 1997